Quantum Associative Memory with a Single Driven-Dissipative Nonlinear Oscillator

Adrià Labay-Mora⬤,[*] Roberta Zambrini⬤, and Gian Luca Giorgi⬤
Institute for Cross Disciplinary Physics and Complex Systems (IFISC) UIB-CSIC, Campus Universitat Illes Balears,
Palma de Mallorca, Spain

Algorithms for associative memory typically rely on a network of many connected units. The prototypical example is the Hopfield model, whose generalizations to the quantum realm are mainly based on open quantum Ising models. We propose a realization of associative memory with a single driven-dissipative quantum oscillator exploiting its infinite degrees of freedom in phase space. The model can improve the storage capacity of discrete neuron-based systems in a large regime and we prove successful state discrimination between n coherent states, which represent the stored patterns of the system. These can be tuned continuously by modifying the driving strength, constituting a modified learning rule. We show that the associative-memory capability is inherently related to the existence of a spectral separation in the Liouvillian superoperator, which results in a long timescale separation in the dynamics corresponding to a metastable phase.

Artificial neural networks (ANNs) are brain-inspired computational systems that can solve and model numerous kinds of tasks, ranging from pattern and speech recognition [1,2] to big data analysis [3]. An important family of ANNs is given by attractor networks, whose temporal evolution settles on stable solutions, exploited in a wide range of problems [4,5] with the prominent example of associative memory (AM). In an AM task, a system stores a set of memory states. Then, it is interrogated using a clue state similar but not necessarily identical to one of the memories; a system equipped with AM can identify the stored pattern most similar to the clue according to a properly defined distance. AMs are commonly modeled through the (classical) Hopfield neural network (HNN) [6], which makes use of a network of binary neurons, and exhibits stable attractors—the memories—defined through a proper *learning rule* written in the weights of the neural connections [4,5]. One main limitation of the HNN is that the number of patterns that can be stored is much smaller than the dimension of the network itself [7,8].

Quantum machine learning aims to find ways to exploit the features of quantum mechanics for machine learning purposes [9–12]. In the context of quantum AM, generalizations of classical models are mainly based on the quantized version of the HNN [13–21], where binary systems are replaced by quantum spins, and where the necessary dissipative dynamics are provided by the interaction with some external bath (which can also encode the learning rule [22,23]). The main findings concern the existence of dynamical phases, not found in classical systems, that can be employed in new types of retrieval. Yet, memories remain strings of classical bits. Still, an open point is the promise that the richer dynamics of quantum

systems can improve the storage capacity, that is, the number of memories over the system size. A general discussion about the possibility of achieving such a quantum advantage can be found in [24,25], where the storage capacity is estimated according to the Gardner program [26,27]. However, direct application to specific models does not seem to give conclusive answers [28,29].

In this Letter, we take an alternative route to AM in quantum systems moving from spin networks to a single driven-dissipative nonlinear quantum oscillator where one can exploit its (in principle infinite) number of degrees of freedom. The main ingredient of our approach lies in the nonlinearity which determines the form and phase symmetry of the steady state, changing from (almost classical) coherent states to purely quantum states, depending on the model parameters. Together with a metastable dynamical phase long enough compared to all timescales relevant to pattern recognition and memory retrieval. Concerning AMs, metastability allows systems that converge towards a unique steady state to span a manifold of relevant addressable memories [30].

In principle, a quantum oscillator spans an infinite Hilbert space with potentially unlimited storage capacity [24]. This can be seen as a (generally complex) network whose computational nodes can be built using every orthogonal basis of the Liouville space (a similar approach was taken in Ref. [31] in the context of quantum reservoir computing). Nevertheless, we are bounded by the size of the metastable manifold. Considering the minimum Hilbert space size needed to correctly describe the system dynamics, we will show that our model can achieve a higher storage capacity than the (classical and quantum) discrete neuron models.

Let us briefly review the concept of metastability, which emerges whenever disparate timescales are present in the evolution of a dynamical system [30]. In our case, as we will see, metastability can be traced back to the presence of a separation in the Liouvillian spectrum [32,33] and is in close connection with quantum entrainment and dissipative phase transitions [34]. It is characterized by the long-lived occupation of high Liouvillian modes and is normally observed after a short transient time and before the final relaxation towards the steady state.

For a system described by the Gorini-Kossakowski-Sudarshan-Lindblad master equation $\partial_t \rho = \mathcal{L}\rho$ [35,36], the dynamics can be understood in terms of the set of complex eigenvalues $\{\lambda_j\}$ of the (non-Hermitian) Liouvillian superoperator $\mathcal{L}$ and of the right ($\{R_j\}$) and left ($\{L_j\}$) eigenvectors, obeying, respectively, $\mathcal{L}R_j = \lambda_j R_j$ and $\mathcal{L}^\dagger L_j = \lambda_j^* L_j$ with normalization $\mathrm{tr}L_j^\dagger R_k = \delta_{jk}$ [32]. Then, assuming the presence of at least one steady state ρ_{ss} (which is always true in finite dimensions [37,38]), the time evolution of a state $\rho(0)$ can be decomposed as

$$\rho(t) = \rho_{ss} + \sum_{j>1} \mathrm{tr}\left[L_j^\dagger \rho(0)\right] e^{\lambda_j t} R_j, \quad (1)$$

where for convenience the eigenvalues are sorted such that $0 \geq \mathrm{Re}\lambda_j \geq \mathrm{Re}\lambda_{j+1}$.

A metastable dynamical phase will emerge before the final relaxation whenever there is a large separation between two consecutive eigenvalues, i.e., $\tau_n \gg \tau_{n+1}$, where $\tau_n^{-1} = -\mathrm{Re}\lambda_n$ [33]. This divides the decay into different timescales: a fast regime for $t < \tau_{n+1}$, a metastable period where dynamics are apparently frozen for $\tau_{n+1} < t < \tau_n$; and, finally, the last decay for $t > \tau_n$. In the middle region, the dynamics can be approximated by $\rho(t) = \sum_{l=1}^{n} p_l(t)\mu_l$ [39], where $\{\mu_l\}_{l=1}^{n}$ are the metastable states spanning the metastable manifold [40] and $\{p_l(t)\}_{l=1}^{n}$ are quasiprobabilities, as they might take negative values, but satisfy that their sum is 1.

Our quantum model for AM consists of a driven-dissipative oscillator described by the master equation

$$\frac{\partial \rho}{\partial t} = -i[\hat{H}_n, \rho] + \gamma_1 \mathcal{D}[\hat{a}]\rho + \gamma_m \mathcal{D}[\hat{a}^m]\rho, \quad (2)$$

where we have standard terms for linear (single-photon) and nonlinear (multiphoton) damping [47,48] with rates γ_1 and γ_m, respectively. The Hamiltonian, which contains a n-order squeezing drive [49,50], in the rotation frame and after the parametric approximation is

$$\hat{H}_n = \Delta\hat{a}^\dagger\hat{a} + i\eta[\hat{a}^n e^{i\theta n} - (\hat{a}^\dagger)^n e^{-i\theta n}]. \quad (3)$$

Here, $\Delta = \omega_0 - \omega_s$ is the detuning between the natural oscillator frequency and that of the squeezing force, η and θ the magnitude and phase of the driving, respectively.

We observe that the model possesses $\mathbb{Z}_n$ symmetry, that is, the transformation $\hat{a} \to \hat{a}\exp(i2\pi/n)$ leaves the master equation invariant [51].

Although particular solutions have been found for specific cases [34,52], no general analytical solution exists for Eq. (2). We can restrict to the case $m = n$ and write it as [47,53,54]

$$\frac{\partial \rho}{\partial t} = -i\Delta[\hat{a}^\dagger\hat{a}, \rho] + \gamma_1\mathcal{D}[\hat{a}]\rho + \gamma_n\mathcal{D}[\hat{a}^n - \beta^n]\rho, \quad (4)$$

where $\beta^n = 2\eta e^{i\theta n}/\gamma_n$ corresponds to the amplitude of n symmetrically distributed coherent states or *lobes*

$$|\beta_j\rangle = |\beta e^{i(2j+1)\pi/n}\rangle, \quad j = 1, ..., n, \quad (5)$$

which span the kernel of the nonlinear damping term in Eq. (4). We notice that β is a function of the ratio between squeezing strength and nonlinear damping. In the limit of small detuning and large β, we observe numerically that the lobes become almost orthogonal ($F(\beta) = |\langle\beta_j|\beta_{j+1\mathrm{mod}n}\rangle|^2 \to 0$), and thus the steady state can be well approximated by $\rho_{ss} \approx (1/n)\sum_{j=1}^{n}|\beta_j\rangle\langle\beta_j|$ [55]. Instead, in the absence of squeezing in Eq. (3), only a single solution with $\beta = 0$ persists. In the following, we fix $\theta = 0$ and $\Delta = 0.4\gamma_1$.

By numerically solving the steady state equation $\mathcal{L}\rho_{ss} = 0$, we show in Fig. 1 its Wigner representation for four different parameter choices [56]. In the first row, we can see two different situations for $n = m = 3$: in panel (a) we have set $\eta \ll \Delta$, which makes the lobes indistinguishable, while for $\eta > \Delta$ [panel (b)] we can appreciate three coherent states corresponding to an amplitude $\beta \sim 3$. The separation between these two regimes could also be observed at the mean-field level, as explicitly discussed in [40] (Sec. S1). Finally, in Fig. 1(c), we show the steady state for $n = 3$ and $m = 2$. Here, we again see three lobes, as expected from the symmetry of the system, but now show signatures of squeezing and quantumness. This also applies to other values of $n \neq m$. In all situations, the Wigner representation is non-negative as a consequence of the linear damping which removes the coherences between states [55,59].
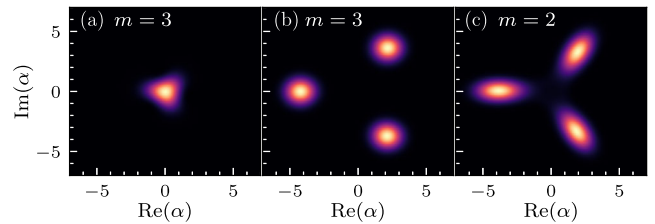
FIG. 1. Wigner representation of the steady state for $n = 3$ (normalized). Parameters: (a) $\gamma_2/\gamma_1 = 0.2$, $\eta/\gamma_1 = 0.1$; (b) $\gamma_2/\gamma_1 = 1.5$, $\eta/\gamma_1 = 2.7$; (c) $\gamma_2/\gamma_1 = 0.2$, $\eta/\gamma_1 = 1.455$.
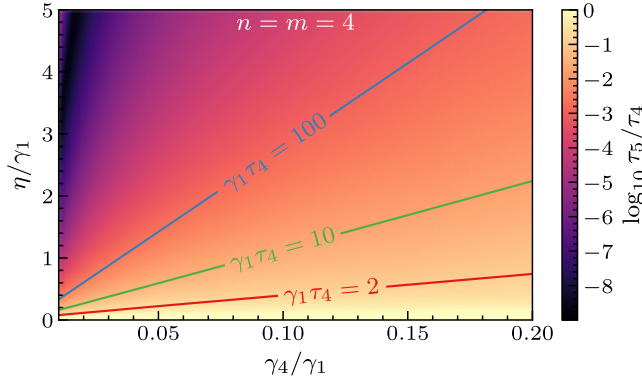
FIG. 2. Separation between the 4th and 5th low-lying eigenvalues where darker colors indicate longer metastability. Three contour lines show the decay time of the fourth eigenvalue, the end of metastability.

FIG. 3. Time evolution of $|\langle \hat{a} \rangle|$ for three different parameter sets as shown in Fig. 2. Full master equation evolution in solid lines (for truncated Hilbert space with dim $\mathcal{H} = 50$) and deterministic evolution in the metastable manifold in dotted lines. Shaded areas indicate the metastability regime per color.

To establish the existence of metastability, let us explore how the separation of the Liouvillian eigenvalues depends on the system parameters. An example is given in Fig. 2 (for $n = m = 4$). There, the separation appears between the fourth and fifth eigenvalues, which separates slow metastable dynamics from fast decay modes [33]. During the slow phase, the dynamics can be approximated by n metastable phases $\{\mu_j\}_{j=1}^{n}$, constructed as extreme superpositions of the first n eigenmodes [40] (Sec. S3). These, in the regime of large β, are approximately equal to the coherent states in Eq. (5). The larger the separation, the farther apart the lobes are, increasing the metastable properties [60].

The results above are consistent with particular situations studied in the literature. Concretely, the case $n = m = 2$ was studied in Ref. [34] using linear amplification instead of linear damping (the presence of both damping and amplification was analyzed in Ref. [62] in the context of quantum synchronization). The change, motivated by its experimental feasibility [47,61,63], leads to a slight increase in metastability because there is no competition between dissipative terms. Yet, no other qualitative difference is appreciated.

We now turn our attention to the dynamic properties that lead to the AM capabilities of the system. Our goal is to exploit the metastable dynamics to discriminate between the n metastable phases. This can be seen as a generalized discrimination problem between n symmetrical coherent states [64,65] because the initial state does not have to be any of the lobes. More specifically, within the metastable transient, an initial state will move towards the closest lobe (representing one of the stored memories) and remain there for a long time. Consequently, by measuring the state within this regime, we can extract information about the corresponding lobe. Furthermore, the ability to tweak the target states using the (tunable) Liouvillian parameters can be interpreted as a modified learning rule, commonly given in ANN by changing the network weights to select the desired family of steady states [6].

In Fig. 3, we compute the time evolution of $\langle \hat{a} \rangle$ for three different values of the parameters (γ_n, η) corresponding to $\gamma_1 \tau_n = \{2, 10, 100\}$. The initial state is a coherent state with amplitude $0.5\beta(\gamma_n, \eta) \exp(i2\pi/9)$, different from any lobe. Then, the evolution is evaluated by comparing the full master equation (solid lines) with the metastable approximation described in Ref. [39] (dotted lines), which, of course, is expected to be valid since the metastable transient.

Looking at the upper two lines, for both n, we can distinguish the different dynamical regimes. First, a fast decay of the high modes (i.e., $R_{j>n}$) occurs, which takes the state from its initial amplitude to that of the lobes in a time τ_{n+1}. Here, as expected, the metastable approximation fails to describe the dynamics. Then, the solution penetrates into the metastable transient where a plateau of constant amplitude is observed. From this point onwards, the two descriptions coincide with high accuracy, showing that the state is confined to the metastable manifold. Thus, in this setting, metastability is completely described by the Liouvillian spectrum. In contrast, when the separation between lobes is small (lower red lines), the metastable transient disappears. We can also appreciate a longer plateau for $n = 4$ than for $n = 3$, even after the metastable transient, which is a consequence of the slowest eigenvalues distribution [40] (Sec. S4).

Next, we assess the AM efficiency by numerically computing the probability that the system is found in the target lobe at each time t. We use a Monte Carlo simulation with a coherent state of random amplitude $[0, 2\beta]$ and phase as initial state. The system is then measured with the (ambiguous) POVM $\{P_k\}_{k=1}^{n}$, obtained numerically from the Liouvillian left eigenmodes [39], where each operator corresponds to a division of the phase space centered around each lobe (5) [66]. Hence, the success probability is equal to the click probability of the kth operator assuming the initial state is most similar to the kth lobe (according to trace distance) [40] (Sec. S5). We repeat this process

400 times with different initial states and average the results to obtain the solid lines in Fig. 4(a).

Focusing on the dim $\mathcal{H}_{\text{eff}} = 40$ (solid red) line, the time evolution can be compared to the metastable evolution in Fig. 3 with a plateau of high success probability that spans times even before the metastable regime begins. This is because any state in the basin of attraction of the lobe will trigger the associated operator, failing to determine whether the state has converged to the exact pattern. Thus, we repeat the calculation with a second (unambiguous) POVM, used experimentally for m-ary phase-shifted keys [67,68], that only triggers when the state is inside the metastable manifold. As a result, looking at the dashed lines in Fig. 4(a), we note that the success probability is initially small—the state is not over any lobe—but converges to the plateau by the start of the metastable transient, thus showing its ability to optimally discriminate the patterns in this regime.

A fundamental question in the context of AM concerns the storage capacity α_c of a system. While our model has an infinitely dimensional Hilbert space, the coherent-state solutions discussed so far can be described with high accuracy by truncating above high Fock state occupancy of the boson mode [50]. This allows us to adapt the definition of the storage capacity of finite systems. In Fig. 4(a), we show the effect of truncation on the lobe identification. As expected, under a certain system size, the dynamical state cannot be well approximated and metastability is lost, which leads to a fast decrease in the success probability. The dimension of the truncated Hilbert space $\mathcal{H}_{\text{eff}}$ represents the effective system size to be compared with the number of stored memories. Assuming that n patterns can be successfully stored, one can define the storage capacity as $\alpha_c = n/\dim\mathcal{H}_{\text{eff}}$. However, the possibility to distinguish them can be strongly hindered depending on the parameter choice [69]. This highlights the importance of accounting for correlations between patterns [26,29]. Hence, we define $\tilde{\alpha}_c = [1 - F(\beta)]\alpha_c$, with $F(\beta)$ as specified above, which vanishes for indistinguishable lobes ($\beta \to 0$) and large dimensions ($\beta \to \infty$) but is maximal for intermediate amplitudes. In Fig. 4(b), we plot the storage capacity as a function of the lobe amplitude for different values of n. Although contrasting different learning rules is not immediate, we compare it with the standard Hebbian rule which has been found to limit the capacity in both classical [7] and quantum [21]. In this way, we can appreciate a wide range of solutions where such classical limit is exceeded [70]. Further, in Fig. 4(c), we show how the maximal storage capacity of our model reduces the system size required to store the same number of patterns in a Hebbian-based HNN.

In this Letter, we have proposed a different approach to AM considering a single driven-dissipative quantum nonlinear oscillator. We have shown that it allows for successful state discrimination during the metastable regime.
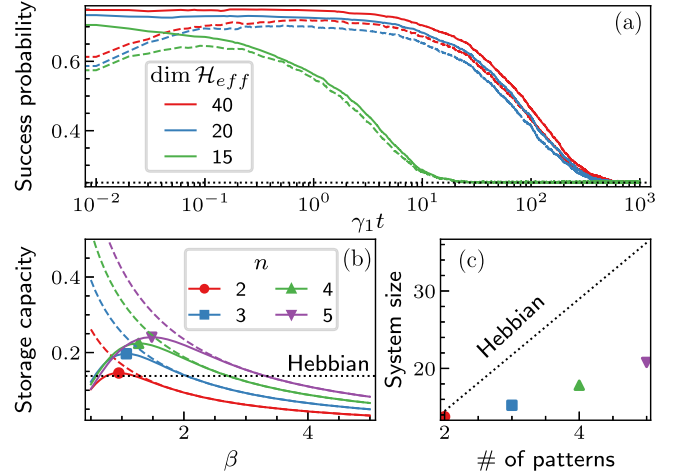
FIG. 4. (a) Probability of identifying the correct lobe with time using the ambiguous (solid lines) and unambiguous (dashed lines) strategies for increasing system sizes. Parameters corresponding to the green line in Fig. 2(b). (b) Storage capacity over lobe amplitude for a different number of patterns: $\tilde{\alpha}_c$ (solid lines) and α_c (dashed lines). (c) Points corresponding to the maximal storage capacity in (b). Compared with Hebbian critical capacity $\alpha_c^{\text{Hebb}} = 0.138$ (dotted line).

Our approach shares some features with the classical continuum space limit of the Wilson-Cowan model [72], whose stochastic versions [73,74] account for metastable neural population activity. In this sense, the Wigner function plays the role of a neural field whose excitations represent the stored patterns [40] (Sec. S7). In contrast to these models where the solutions settle at long times, our AM is transient, which may provide a speed-up in the convergence towards the patterns [75].

Even if bosonic models can potentially encode an infinite number of memories [76], our system is upper-bounded by two values: the power of the nonlinear term n and the overlap between the lobes $F(\beta)$. The latter is similar to the conditions for patterns in HNNs, which require them to be orthogonal. At the same time, the former determines the dimension of the metastable manifold, i.e., the number of metastable solutions. In this respect, we saturate the maximum number of patterns of the system [24], and most importantly, n is not upper bounded in theory.

We can compare our proposal, where the number of solutions can be increased with the nonlinearity degree n, with the standard Hebbian learning strategy, where one needs to increase the dimension of the Hilbert space (number of spins). As the former can be well approximated by truncation, we have found a superior storage capacity $\tilde{\alpha}_c > \alpha_c^{\text{Hebb}}$. Furthermore, truncation saves computational resources and time, and more importantly, in experimental realizations, its validity witnesses a bound in the maximum excited state and thus in the operation energy [Fig. 4(c)]. In any case, the experimental viability of our system mainly depends on the capacity to engineer an oscillator with a

high nonlinear term. Superconducting resonators are a good candidate when $n = m$ due to their ability to realize any nonlinearity by modifying only the flux pump frequency [50,63] with three-photon down-conversion achieved in Ref. [77]. Those systems have been used to generate catlike states by removing the linear dissipative term [47]. Consequently, the appearance of the linear term makes it easier to realize in practice. Aside, experiments realizing the phase-shifted coherent state discrimination have been pursued with success [68].

To conclude, we believe this Letter heralds a new way of pursuing AM beyond typical spin chains. It would be interesting to see the robustness and scalability of this proposal when coupling a few nonlinear oscillators. More complex metastability scenarios where the spectral analysis is not sufficient could arise, e.g., in the presence of skin and topological effects [78–80]. Also, in Ref. [34], it was shown that the onset of metastability relates to an exceptional point in the Liouvillian spectrum of the van der Pol oscillator. This and other dynamical aspects need to be further explored. An additional open question concerns the possibility of storing *quantum memories*. While for the sake of clarity in this work we have focused on the case $n = m$, which is built around coherent-state discrimination, Fig. 1(c) shows that in different scenarios metastable squeezed states can emerge. This aspect is left for future work.

---

[*]alabay@ifisc.uib-csic.es

[1] S.-I. Amari, Neural Comput. **10**, 251 (1998).

[2] C. M. Bishop, Mach. Learn. **128** (2006).

[3] G. E. Hinton and R. R. Salakhutdinov, *Pattern Recognition and Machine Learning* (Springer, New York, 2006).

[4] D. J. Amit, *Modeling Brain Function: The World of Attractor Neural Networks* (Cambridge University Press, Cambridge, England, 1989).

[5] J. Hertz, A. Krogh, and R. G. Palmer, *Introduction to the Theory of Neural Computation* (CRC Press, Boca Raton, 2018).

[6] J. J. Hopfield, Proc. Natl. Acad. Sci. U.S.A. **79**, 2554 (1982).

[7] D. J. Amit, H. Gutfreund, and H. Sompolinsky, Phys. Rev. Lett. **55**, 1530 (1985).

[8] D. J. Amit, H. Gutfreund, and H. Sompolinsky, Ann. Phys. (N.Y.) **173**, 30 (1987).

[9] P. Wittek, *Quantum Machine Learning: What Quantum Computing Means to Data Mining* (Academic Press, New York, 2014).

[10] J. Biamonte, P. Wittek, N. Pancotti, P. Rebentrost, N. Wiebe, and S. Lloyd, Nature (London) **549**, 195 (2017).

[11] V. Dunjko and H. J. Briegel, Rep. Prog. Phys. **81**, 074001 (2018).

[12] G. Carleo, I. Cirac, K. Cranmer, L. Daudet, M. Schuld, N. Tishby, L. Vogt-Maranto, and L. Zdeborová, Rev. Mod. Phys. **91**, 045002 (2019).

[13] S. Gopalakrishnan, B. L. Lev, and P. M. Goldbart, Philos. Mag. **92**, 353 (2012).

[14] M. C. Diamantini and C. A. Trugenberger, Phys. Rev. Lett. **97**, 130503 (2006).

[15] S. Gopalakrishnan, B. L. Lev, and P. M. Goldbart, Phys. Rev. Lett. **107**, 277201 (2011).

[16] V. Torggler, S. Krämer, and H. Ritsch, Phys. Rev. A **95**, 032310 (2017).

[17] P. Rotondo, M. Marcuzzi, J. P. Garrahan, I. Lesanovsky, and M. Müller, J. Phys. A **51**, 115301 (2018).

[18] P. Rebentrost, T. R. Bromley, C. Weedbrook, and S. Lloyd, Phys. Rev. A **98**, 042308 (2018).

[19] F. Carollo and I. Lesanovsky, Phys. Rev. Lett. **126**, 230601 (2021).

[20] E. Fiorelli, I. Lesanovsky, and M. Müller, New J. Phys. (2022).

[21] B. P. Marsh, Y. Guo, R. M. Kroeze, S. Gopalakrishnan, S. Ganguli, J. Keeling, and B. L. Lev, Phys. Rev. X **11**, 021048 (2021).

[22] P. Rotondo, M. Cosentino Lagomarsino, and G. Viola, Phys. Rev. Lett. **114**, 143601 (2015).

[23] E. Fiorelli, M. Marcuzzi, P. Rotondo, F. Carollo, and I. Lesanovsky, Phys. Rev. Lett. **125**, 070604 (2020).

[24] M. Lewenstein, A. Gratsea, A. Riera-Campeny, A. Aloy, V. Kasper, and A. Sanpera, Quantum Sci. Technol. **6**, 045002 (2021).

[25] L. Bödeker, E. Fiorelli, and M. Müller, arXiv:2210.07894.

[26] E. Gardner, J. Phys. A **21**, 257 (1988).

[27] E. Gardner and B. Derrida, J. Phys. A **21**, 271 (1988).

[28] A. Gratsea, V. Kasper, and M. Lewenstein, arXiv:2111.08414.

[29] F. Benatti, G. Gramegna, and S. Mancini, J. Phys. A, **55** 155301 (2022).

[30] B. A. Brinkman, H. Yan, A. Maffei, I. M. Park, A. Fontanini, J. Wang, and G. La Camera, Appl. Phys. Rev. **9**, 011313 (2022).

[31] L. C. G. Govia, G. J. Ribeill, G. E. Rowlands, H. K. Krovi, and T. A. Ohki, Phys. Rev. Res. **3**, 013077 (2021).

[32] F. Minganti, A. Biella, N. Bartolo, and C. Ciuti, Phys. Rev. A **98**, 042118 (2018).

[33] K. Macieszczak, M. Guţă, I. Lesanovsky, and J. P. Garrahan, Phys. Rev. Lett. **116**, 240404 (2016).

[34] A. Cabot, G. L. Giorgi, and R. Zambrini, New J. Phys., **23** 103017 (2021).

[35] G. Lindblad, Commun. Math. Phys. **48**, 119 (1976).

[36] V. Gorini, A. Kossakowski, and E. C. G. Sudarshan, J. Math. Phys. (N.Y.) **17**, 821 (1976).

[37] D. E. Evans and H. Hanche-Olsen, J. Funct. Anal. **32**, 207 (1979).

[38] B. Baumgartner and H. Narnhofer, J. Phys. A **41**, 395303 (2008).

[39] K. Macieszczak, D. C. Rose, I. Lesanovsky, and J. P. Garrahan, Phys. Rev. Res. **3**, 033047 (2021).

[40] See Supplemental Material at http://link.aps.org/supplemental/10.1103/PhysRevLett.130.190602 for details on analytical calculations, which includes Refs. [41–46].

[41] T. Rudolph, R. W. Spekkens, and P. S. Turner, Phys. Rev. A **68**, 010301(R) (2003).

[42] R. Azouit, A. Sarlette, and P. Rouchon, in *2015 54th IEEE Conference on Decision and Control (CDC)* (IEEE, New York, 2015), pp. 6447–6453.

[43] R. Azouit, A. Sarlette, and P. Rouchon, ESAIM Control Optim. Calc. Var. **22**, 1353 (2016).

[44] C. Chamberland, K. Noh, P. Arrangoiz-Arriola, E. T. Campbell, C. T. Hann, J. Iverson, H. Putterman, T. C. Bohdanowicz, S. T. Flammia, A. Keller *et al.*, PRX Quantum **3**, 010329 (2022).

[45] E. C. S. Meccia and R. P. Perazzo, Neural Process. Lett. **16**, 243 (2002).

[46] H. J. Carmichael, *Statistical Methods in Quantum Optics 1: Master Equations and Fokker-Planck Equations*, Vol. 1 (Springer Science & Business Media, New York, 1999).

[47] S. O. Mundhada, A. Grimm, S. Touzard, U. Vool, S. Shankar, M. H. Devoret, and M. Mirrahimi, Quantum Sci. Technol. **2**, 024005 (2017).

[48] S. Gevorkyan and V. Chaltykyan, J. Mod. Opt. **46**, 1447 (1999).

[49] S. L. Braunstein and R. I. McLachlan, Phys. Rev. A **35**, 1659 (1987).

[50] B. Lang and A. D. Armour, New J. Phys. **23**, 033021 (2021).

[51] F. Minganti, V. Savona, and A. Biella, arXiv:2303.03355.

[52] N. Bartolo, F. Minganti, W. Casteels, and C. Ciuti, Phys. Rev. A **94**, 033841 (2016).

[53] M. Mirrahimi, Z. Leghtas, V. V. Albert, S. Touzard, R. J. Schoelkopf, L. Jiang, and M. H. Devoret, New J. Phys. **16**, 045014 (2014).

[54] W.-L. Ma, S. Puri, R. J. Schoelkopf, M. H. Devoret, S. Girvin, and L. Jiang, Sci. Bull. **66**, 1789 (2021).

[55] S. T. Gevorgyan, M. Xiao, and V. O. Chaltykyan, J. Mod. Opt. **55**, 1923 (2008).

[56] All the results presented have been obtained numerically using QuTip [57] and QuantumOptics.jl [58], code available at https://gitlab.ifisc.uib-csic.es/quantum/.

[57] J. Johansson, P. Nation, and F. Nori, Comput. Phys. Commun. **184**, 1234 (2013).

[58] S. Krämer, D. Plankensteiner, L. Ostermann, and H. Ritsch, Comput. Phys. Commun. **227**, 109 (2018).

[59] L. Gilles, B. M. Garraway, and P. L. Knight, Phys. Rev. A **49**, 2785 (1994).

[60] This is in correspondence with the results found in Ref. [61] where squeezing reduces the effects of noise and enhances the stability of the lobes.

[61] S. Sonar, M. Hajdušek, M. Mukherjee, R. Fazio, V. Vedral, S. Vinjanampathy, and L.-C. Kwek, Phys. Rev. Lett. **120**, 163601 (2018).

[62] W.-K. Mok, L.-C. Kwek, and H. Heimonen, Phys. Rev. Res. **2**, 033422 (2020).

[63] I.-M. Svensson, A. Bengtsson, J. Bylander, V. Shumeiko, and P. Delsing, Appl. Phys. Lett. **113**, 022602 (2018).

[64] R. Nair, B. J. Yen, S. Guha, J. H. Shapiro, and S. Pirandola, Phys. Rev. A **86**, 022306 (2012).

[65] S. Izumi, M. Takeoka, K. Ema, and M. Sasaki, Phys. Rev. A **87**, 042328 (2013).

[66] N. Lörch, Y. Zhang, C. Bruder, and M. I. Dykman, Phys. Rev. Res. **1**, 023023 (2019).

[67] S. Izumi, M. Takeoka, M. Fujiwara, N. D. Pozza, A. Assalini, K. Ema, and M. Sasaki, Phys. Rev. A **86**, 042328 (2012).

[68] F. Becerra, J. Fan, G. Baumgartner, J. Goldhar, J. Kosloski, and A. Migdall, Nat. Photonics **7**, 147 (2013).

[69] For instance, as we saw in Fig. 1(a), a one lobe solution is present with $n = 3$ with β small, implying a small effective dimension and, consequently, a high storage capacity [40] (Sec. S6).

[70] We note that the Hebbian critical capacity is found in the limit of infinite dimension (neurons) and zero temperature while in our case the dimension is finite once the Hilbert space is truncated. Nevertheless, the critical value seems to apply to finite resources too. For instance, Marsh *et al.* [21] found numerically that this limit persists with at least 200 neurons, and practical examples never overcome this limit [23,71].

[71] A. Fuchs and H. Haken, Biol. Cybern. **60**, 17 (1988).

[72] H. R. Wilson and J. D. Cowan, Biophys. J. **12**, 1 (1972).

[73] M. A. Buice and J. D. Cowan, Phys. Rev. E **75**, 051919 (2007).

[74] P. C. Bressloff, Phys. Rev. E **82**, 051903 (2010).

[75] E. Fiorelli, P. Rotondo, M. Marcuzzi, J. P. Garrahan, and I. Lesanovsky, Phys. Rev. A **99**, 032126 (2019).

[76] E. C. Segura and R. P. Perazzo, Neural Process. Lett. **12**, 129 (2000).

[77] C. W. S. Chang, C. Sabín, P. Forn-Díaz, F. Quijandría, A. M. Vadiraj, I. Nsanzineza, G. Johansson, and C. M. Wilson, Phys. Rev. X **10**, 011011 (2020).

[78] T. Haga, M. Nakagawa, R. Hamazaki, and M. Ueda, Phys. Rev. Lett. **127**, 070402 (2021).

[79] T. Mori, Phys. Rev. Res. **3**, 043137 (2021).

[80] V. P. Flynn, E. Cobanera, and L. Viola, Phys. Rev. Lett. **127**, 245701 (2021).